Fundamental diagram in the context of the Social Force Model

I.M. Sticco,[1] G.A. Frank,[2] F.E. Cornes,[1] and C.O. Dorso[1, 3]

[1]*Departamento de Física, Facultad de Ciencias Exactas y Naturales, Universidad de Buenos Aires, Pabellón I,*
Ciudad Universitaria, 1428 Buenos Aires, Argentina.
[2]*Unidad de Investigación y Desarrollo de las Ingenierías, Universidad Tecnológica Nacional Facultad Regional Buenos Aires,*
Av. Medrano 951, 1179 Buenos Aires, Argentina.
[3]*Instituto de Física de Buenos Aires, Pabellón I, Ciudad Universitaria, 1428 Buenos Aires, Argentina.*
(Dated: December 12, 2018)

The fundamental diagram of pedestrian dynamics gives the relation between the density and the flow in a specific enclosure. It is characterized by two distinctive behaviors: the free-flow regime (for low densities) and the congested regime (for high densities). In the former, the flow is an increasing function of the density, while on the latter, the flow does not increase. In this work we perform numerical simulations of the pilgrimage of the entrance to the Jamaraat bridge (pedestrians walking along a straight corridor) and compare flow-density measurements with empirical measurements made by Helbing et al. We show that under high density conditions, the Social Force Model is not capable of reproducing the fundamental diagram reported in empirical measurements. We use analytical techniques and numerical simulations to prove that with an appropriate modification of the friction coefficient it is possible to attain the qualitative behavior of the expected flow-density relation. Other authors proposed a modification of the relaxation time in order to address this problem. In this work, we unveil the fact that our approach is analogous to theirs, since both affect the same term of the reduced-in-units equation of motion. We inspect how the friction modification affects the pedestrian clustering structures present in the transition from the free-flow regime to the congested regime. We also discover that the speed profile, normalized by width and maximum velocity yield a universal behavior regardless the corridor dimensions.

I. INTRODUCTION

By the late '90s and the beginning of the century, Helbing and co-workers postulated that either the environment and the individuals' own desire affect the pedestrians motion in a similar way as forces do with respect to the momentum of particles [1, 2]. This "social force model" (SFM) nicely bridged the socio-psychological phenomenon of crowds behavior to the "microscopic" formalism of moving particles. The model succeeded at this instance to explain why the crowd evacuation slows down as pedestrians try harder to escape from a dangerous situation (*i.e.* "faster is slower" effect) [1, 3, 4].

The SFM, in its basic version, was reported to be suitable for a variety of panic situations, including the presence of obstacles, or the existence of more than one exit [5, 6]. More sophisticated scenarios required, however, a step up implementation [7–9], although sustaining the basic model and its parameters.

Some questioning arose, on the true psychological tendency of the pedestrians to stay away from each other. While the social forces accomplish this tendency, it attains a somewhat unrealistic "colliding behavior" for slowly moving pedestrians [10]. His (her) repulsive tendency is expected to decrease as approaching a more crowded environment. The small fall-off length $B = 0.08$ m suggested by Helbing in Ref. [1] does not

completely solve this issue. It neither agrees with the fact that pedestrians prefer to keep a comfortable 0.5 m distance between each other in a moderately crowded environment, nor it fits accurately the empirical velocities reported for non-panicking crowds [10].

Researchers turned back to examine the available data on the velocity and flux behavior for different density environments [11–13]. Ref. [11] is a wonderful summary of empirical data from literature, and their own data set, acquired from videos of the Muslim pilgrimage in Mina-Makkah (2006). They showed from the empirical fundamental diagram (flux J versus density ρ) that highly dense crowds (seemingly up to 10 p/m^2) do not drive the pedestrians velocity to zero, although the reasons for this remain rather obscure.

The high density regime appears to be the most cumbersome one. Caution was claimed when (automatically) transferring the usual "calibrated" parameters of the SFM to this regime. It was argued that the pedestrians' body size distribution and the "situational context" is somewhat responsible for the unexpected departure from these parameters [14, 15]. But other researchers pointed out that this departure actually expresses the lack of a mechanism to properly handle the pedestrians' "required space to move". Some modifications to the basic SFM were then proposed to overcome this difficulty [16, 17].

Although a mechanism allowing an "increase of the space to move" (due to the fear of crushing or injury)

is a compelling necessity in the context of the SFM, a sharp "re-calibration" of the model for high density situations appears not to be completely satisfactory [18]. A more "natural" way of handling this matter requires a deep examination of the current SFM parameters. The net-time headway (roughly, the relaxation time) was first examined in Ref. [18]. The author sustains the hypothesis that the pedestrians net-time headway should increase until there is "enough space to make a step". He shows that a density dependent net-time headway is a suitable parameter to smartly reproduce the empirical fundamental diagram for highly dense crowds [18].

Our own examination of the SFM parameters suggests that not only the net-time headway, but the friction between pedestrians (and with the walls) can reproduce the pattern of the fundamental diagram. Our working hypothesis is that friction is the crucial parameter in the dynamics of highly dense crowds. We actually sustain the SFM model with no further "re-calibrations", but with the right friction setting, in order to meet the fundamental diagram pattern.

Our investigation is organized as follows. We first recall the SFM in Section II A, while including the precise definitions for flux, density and clustered structures. Section III presents our numerical simulations for pedestrians moving through corridors. The corresponding results are shown in Section IV. Our main conclusions are detailed in the closing Section V.

II. BACKGROUND

A. The Social Force Model

Our research was carried out in the context of the "social force model" (SFM) proposed by Helbing and co-workers [1]. This model states that human motion is caused by the desire of people to reach a certain destination, as well as other environmental factors. The pedestrians behavioral pattern in a crowded environment can be modeled by three kind of forces: the "desire force", the "social force" and the "granular force".

The "desire force" represents the pedestrian's own desire to reach a specific target position at a desired velocity v_d. But, in order to reach the desired target, he (she) needs to accelerate (decelerate) from his (her) current velocity $\mathbf{v}^{(i)}(t)$. This acceleration (or deceleration) represents a "desire force" since it is motivated by his (her) own willingness. The corresponding expression for this forces is

$$\mathbf{f}_d^{(i)}(t) = m_i \frac{v_d^{(i)} \mathbf{e}_d^{(i)}(t) - \mathbf{v}^{(i)}(t)}{\tau} \qquad (1)$$

where m_i is the mass of the pedestrian i. $\mathbf{e}_d$ corresponds to the unit vector pointing to the target position and τ is a constant related to the relaxation time needed to reach his (her) desired velocity. For simplicity, we assume that v_d remains constant during the entire process and is the same for all individuals, but $\mathbf{e}_d$ changes according to the current position of the pedestrian. Detailed values for m_i and τ can be found in Refs. [1, 5].

The "social force" represents the psychological tendency of two pedestrians, say i and j, to stay away from each other by a repulsive interaction force

$$\mathbf{f}_s^{(ij)} = A_i\, e^{(R_{ij} - r_{ij})/B_i} \mathbf{n}_{ij} \qquad (2)$$

where (ij) means any pedestrian-pedestrian pair, or pedestrian-wall pair. A_i and B_i are fixed values, r_{ij} is the distance between the center of mass of the pedestrians i and j and the distance $R_{ij} = R_i + R_j$ is the sum of the pedestrians radius. $\mathbf{n}_{ij}$ means the unit vector in the $\vec{ji}$ direction.

Any two pedestrians touch each other if their distance r_{ij} is smaller than R_{ij}. Analogously, a pedestrian touch a wall if his/her distance r_{ij} to the wall is smaller than R_i. In these cases, an additional force is included in the model, called the "granular force"(*i.e.* friction force). This force is considered be a linear function of the relative (tangential) velocities of the contacting individuals. In the case of the friction exerted by the wall, the force is a linear function of the tangential velocity. Its mathematical expression reads

$$\mathbf{f}_g^{(ij)} = \kappa\,(R_{ij} - r_{ij})\,\Theta(R_{ij} - r_{ij})\,\Delta\mathbf{v}^{(ij)} \cdot \mathbf{t}_{ij} \qquad (3)$$

where κ is the friction coefficient. The function $\Theta(R_{ij} - r_{ij})$ is zero when its argument is negative (that is, $R_{ij} < r_{ij}$) and equals unity for any other case (Heaviside function). $\Delta\mathbf{v}^{(ij)} \cdot \mathbf{t}_{ij}$ represents the difference between the tangential velocities of the sliding bodies (or between the individual and the walls).

The above forces actuate on the pedestrians dynamics by changing his (her) current velocity. The equation of motion for pedestrian i reads

$$m_i \frac{d\mathbf{v}^{(i)}}{dt} = \mathbf{f}_d^{(i)} + \sum_{j=1}^{N} \mathbf{f}_s^{(ij)} + \sum_{j=1}^{N} \mathbf{f}_g^{(ij)} \qquad (4)$$

where the subscript j represents all the other pedestrians (excluding i) and the walls.

In the original model, there is no distinction between the friction coefficient of pedestrian-pedestrian interaction and pedestrian-wall interaction. Both interactions are modeled with the constant parameter κ. In this paper

we analyze situations in which the friction coefficient may take different values. We define κ_i and κ_w as the friction coefficient related to the pedestrian-pedestrian interaction and the pedestrian-wall interaction respectively.

B. Fundamental Diagram

Inspired in the vehicular traffic dynamic studies, many researches of pedestrian dynamics focus their attention on the relation between the flow and density of a moving crowd. This analysis is called fundamental diagram and it has become one of the most common ways to characterize the pedestrians dynamics along corridors in unidirectional and bidirectional flows [13, 19–22].

In this paper we use the mathematical expressions defined by Helbing et al. in Ref. [11] as regards to the fundamental diagram analysis. Thus, the local density at place $\vec{r} = (x, y)$ and time t is defined as

$$\rho(\vec{r}, t) = \sum_j f(\vec{r}_j(t) - \vec{r}) \qquad (5)$$

where function $f(\vec{r}_j(t) - \vec{r})$ is a Gaussian distance-dependent weight function defined as

$$f(\vec{r}_j - \vec{r}) = \frac{1}{\pi R^2} \exp[-\|\vec{r}_j - \vec{r}\|^2 / R^2] \qquad (6)$$

$\vec{r}_j(t)$ are the positions of the pedestrians j in the surrounding of $\vec{r}$ and R is a measurement parameter. The local speeds have been defined via the weighted average

$$\vec{V}(\vec{r}, t) = \frac{\sum_j \vec{v}_j f(\vec{r}_j(t) - \vec{r})}{\sum_j f(\vec{r}_j(t) - \vec{r})} \qquad (7)$$

while flow have been determined according to the fluid-dynamic formula

$$\vec{J}(\vec{r}, t) = \rho(\vec{r}, t)\vec{V}(\vec{r}, t) \qquad (8)$$

It is well known that the original version of the social force model is incapable of reproducing the fundamental diagram at high densities. Different approaches have been proposed to fix this failure: increasing the net-time headway [18], canceling the desired velocity [16] or even inducing the jamming state by an attraction [15]. These approaches are very useful when individuals do not feel anxious to reach certain destination (*i.e.* non panicking individuals). However, when individuals are escaping or rushing due to a stressful situation, pedestrians would not consider reducing their desired force nor feel the urge to see an attraction.

C. Clustering structures

One of the characteristic feature of pedestrian dynamics is the formation of clusters. Clusters of pedestrians can be defined as the set of individuals that for any member of the group (say, i) there exists at least another member belonging to the same group (j) in contact with the former. Thus, we define a "granular cluster" (C_g) following the mathematical formula given in Ref. [3]

$$C_g : P_i \; \epsilon \; C_g \Leftrightarrow \exists \; j \; \epsilon \; C_g / r_{ij} < (R_i + R_j) \qquad (9)$$

where (P_i) indicate the ith pedestrian and R_i is his/her radius (shoulders width). That means, C_g is a set of pedestrians that interact not only with social and desired force, but also with granular forces (*i.e.* friction forces). The size of the cluster is defined as the number of pedestrians that compose it. The fraction of clustered individuals is defined as the quotient between clustered individuals with respect to the total number of individuals in the crowd. In Section IV E we analyze the clustering structures in terms of these two observables.

III. NUMERICAL SIMULATIONS

The simulations processes were performed on a straight corridor of length $L = 28$ m and variable width size w. We explored different width values ranging from $w = 2$ m to $w = 40$ m. The corridor had two horizontal walls. One of them was placed at $y = 0$ and the other one was placed at $y = w$. The length of each wall was L. The pedestrians were modeled as soft spheres of radius $R_i = 0.23$ m, this size was fixed according to Ref. [23]. Initially, the individuals were randomly distributed along the corridor with a fixed global density and with random initial velocities, resembling a Gaussian distribution with null mean value. We explored global density values in the range $1 < \rho < 9$. The number of pedestrians in the simulation was given by the global density and the corridor dimensions chosen in each case.

The simulations were supported by LAMMPS molecular dynamics simulator with parallel computing capabilities [24]. The time integration algorithm followed the velocity Verlet scheme with a time step of 10^{-4} s. All the necessary parameters were set to the same values as in previous works (see Refs. [6, 25]), except for the friction coefficient κ. In this work we use the original value $\kappa = 2.4 \times 10^5$ and we further utilize $\kappa_i = 2.4 \times 10^6$ and $\kappa_w = 2.4 \times 10^6$, being κ_i and κ_w the pedestrian-pedestrian friction coefficient and the pedestrian-wall friction coefficient respectively.

We implemented special modules in C++ for upgrading the LAMMPS capabilities to attain the social force model simulations. We also checked over the LAMMPS

output with previous computations (see Refs. [3–5, 7, 8]).

The desired velocity for each pedestrian i was $\vec{v}_d^{\,i} = 1$ m/s $\hat{e}_d^{\,i}$, where the target $\hat{e}_d^{\,i}$ was set as $\hat{e}_d^{\,i} = (L, y_i) \, \|(L, y_i)\|^{-1}$, being L the x-location of the end of the corridor and y_i the y-location corresponding to the ith pedestrian. This produced the pedestrians to move from left to right in an unidirectional flow. Pedestrians that overpassed $x = L$ were re-injected in $x = 0$ preserving its current velocity and y-location (*i.e.* periodic boundary conditions). This mechanism was carried out in order to keep the crowd size unchanged.

The measurements were taken once the system reaches the stationary state ($t = 30$ s), the configurations of the systems were recorded every 0.05 s, that is, at intervals as short as 10% of the pedestrians relaxation time (see Sec. II A). The recorded magnitudes were the pedestrians positions and velocities for each process. We also computed the clusterering structures using a LAMMPS built in function.
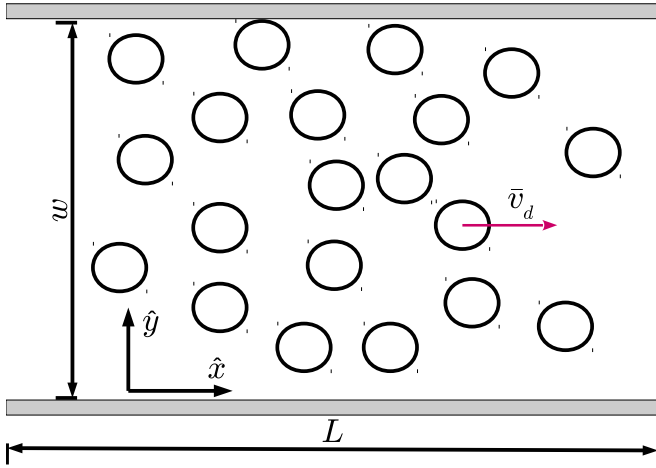

FIG. 1. Schematic diagram for individuals in the corridor. The circles represent pedestrians moving from left to right. w represents the corridor width, L represents the length. The rectangular boxes are the walls of the corridor.

IV. RESULTS

A. Fundamental diagram in the original model

In this subsection we present the results corresponding to the relation of the local flow, velocity and density (*i.e.* fundamental diagram). The measurements were taken in the middle of the corridor using the definitions given in Eq. (8) and Eq. (7). All the results shown here correspond to $R = 1$ m. We tried different values of R and we saw robustness of the results.

In Fig 2, we show the fundamental diagram (density vs. flow) for different corridor widths. We can distinguish the two typical branches of the fundamental diagram. In the free flow branch ($\rho < 5$), the flow increases linearly with the density, since there are no collisions between pedestrians. In this regime, pedestrians achieve the desired velocity, leading to a flow that grows linearly with the density. That is the reason why the flow takes the value of $J \sim \rho$ until $\rho = 5$. This behavior applies to all the corridor width analyzed.

On the other hand, we have the congested branch for $\rho > 5$. Here we face two different scenarios:

- i) In narrow corridors (say $w < 10$) we can see that the flow reduces as the density increases. This resembles the traditional behavior of the fundamental diagram reported in the literature.

- ii) In wide corridors (say $w > 15$) we see that the flow increases with density. This contradicts the typical behavior of the fundamental diagram.

In the case of wide corridors, both the simulated case and the empirical results converge to a constant flow value. It is remarkable that the system does not reach a freezing state such as the one reported in Ref.[15]. We believe that this happens because our simulated agents (as well as the empirical measurements in Ref.[11]) have a well defined target, the respect factor reported in Ref.[16] is negligible due to the circumstances and there is no reason for the individuals to stop.

The inset of the Fig. 2 corresponds to the empirical measures of Helbing et al. at the entrance of the Jamaraat bridge (the corridor width was $w = 22$ m) [11]. Notice that our simulated result corresponding to a $w = 22$ m corridor, exhibit a different behavior in the congested branch. In the simulated case, the flow increases even for the greatest densities. On the contrary, the empirical measurement exhibit a flow reduction for $\rho > 5$ and it reaches a plateau for the highest density values.

In order to satisfy the fundamental diagram reported in the literature, it is necessary that the flow at the maximum density ($\rho_{max} = 9$) be less than the flow at $\rho = 5$. That is: $J(\rho = 9) < J(\rho = 5)$. From the flow definition in Eq. 8 we can derive

$$v(\rho_{max}) < \frac{5v_d}{\rho_{max}}$$
$$v(\rho_{max}) < \frac{5}{9}v_d$$

As our desired velocity is fixed $v_d = 1$ m/s, we conclude that the speed at the maximum density has to be bounded by $v(\rho_{max}) \lesssim 0.5$ m/s in order to satisfy the qualitative behavior of the fundamental diagram

reported in the literature.

The above reasoning is consistent with the speed-density results shown in Fig. 3. As a visual guide we plotted $v = 0.5$ m/s with a horizontal dashed line. Pay attention to the velocity values in $\rho_{max} = 9$. The values corresponding to the wider corridors ($w = 15$ m and $w = 22$ m) both exceed $v = 0.5$ m/s. On the other hand, the values corresponding to narrower corridors fall below $v = 0.5$ m/s.
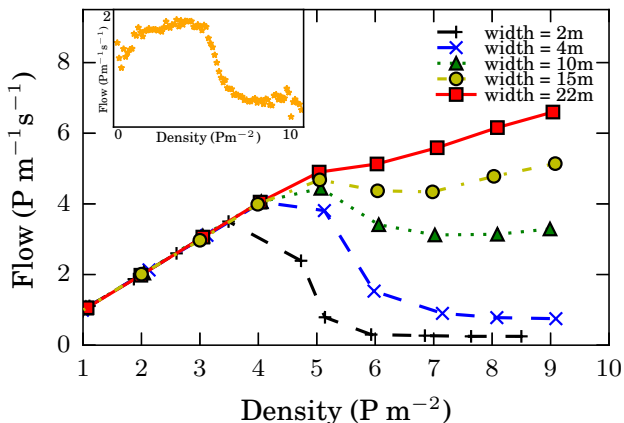

FIG. 3. Speed as a function of the density for different widths. Initially, pedestrians were randomly distributed along the corridor. The measurements were taken in the middle of the corridor once the system reached the stationary state. The length of the corridor was 28 m in all cases with periodic boundary conditions in the x direction.

FIG. 2. Flow as a function of the density for different widths. Initially, pedestrians were randomly distributed along the corridor. The measurements were taken in the middle of the corridor once the system reached the stationary state. The length of the corridor was 28 m in all cases with periodic boundary conditions in the x direction.

The plots in Fig. 3 support the fact that when the density is low enough, pedestrians manage to walk at the desired velocity ($v = 1$ m/s). Only for $\rho > 5$ the velocity begins the slow down proses. The inset shows the measurements at the entrance of the Jamaraat bridge. When comparing our results with the measurements of the Jamaraat bridge, it must be pointed out that the latter do not show a constant velocity for lower densities. We attribute this difference to the fact that in the real system, the pedestrian path are more complex when the density is low. Another interesting finding here is that the wider the corridor, the greater the velocity for all the density values. In Section IV B we will further discuss this topic.

In this subsection we have shown that the original social force model is not capable of reproducing the fundamental diagram since the flow increases even for overcrowded scenarios.
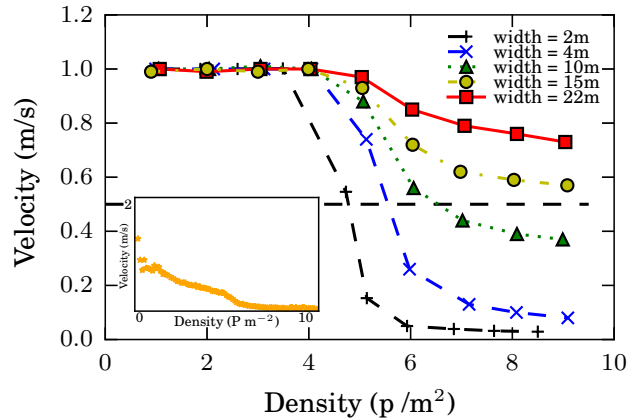
B. Velocity profile

As we mentioned in Section IV A, when the density is low, pedestrians achieve the desired velocity ($v = v_d = 1$ m/s). Since the results of the previous section only hold for the area located in the middle of the corridor, we want to shed some light and understand what is happening in the entire corridor.

In Fig. 4 we show the velocity profile (velocity vs. y-location) of the pedestrians in the corridor. We can see that low-density situations lead to a cruising velocity profile $v = v_d$. This is valid for every location in the corridor (not only the center as was previously proved). For higher densities, the velocity profile turns into a parabola-like function. This shape resembles the typical velocity profile under conditions of laminar flow in a viscous fluid, where the velocity increases toward the center of a tube. In our case, pedestrians near near the walls are the one with the lower velocity. The velocity increases when moving away from the wall until it reaches the maximum in the center of the corridor. This behavior suggests that the friction that the wall exerts on pedestrians, is playing a fundamental role in the velocity distribution. We did some simulations removing the walls and adding periodic boundary conditions in the y-coordinate. This yield to constant-cruising velocity profiles for all the densities, confirming that the walls are a necessary condition in order to produce a parabola-shaped speed profile.

In Fig. 5 we show the velocity profile for different widths. The horizontal axis of the plot corresponds to the y-location normalized by the width of the corridor.
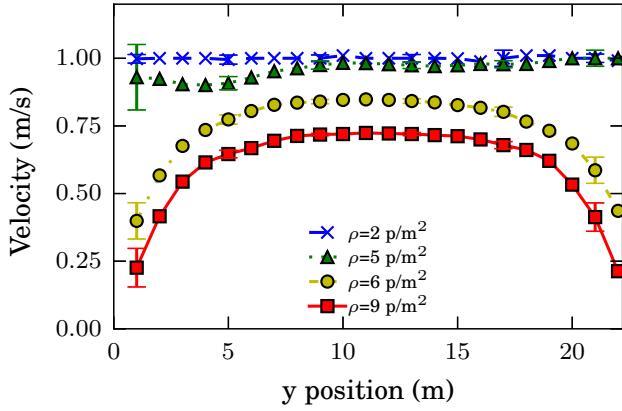
FIG. 4. Velocity profile (velocity vs y-position) for different densities (see legend for the corresponding densities). The simulated corridor was 28 m lenght. Pedestrians walk from left to right with periodic boundary condition in the x-direction. Initially, pedestrians were randomly distributed, the corridor width was $w = 22$ m in all the cases.

The density chosen was $\rho = 6$ since we wanted to study a situation in which pedestrians collide with each other. Remember that when $\rho < 5$, the pedestrians manage to avoid collisions. We can see the parabola shape in which the lowest velocities are in the areas near the walls. There is a clear dependence on v_{max} with the corridor width. It is interesting that the wider the corridor, the higher the maximum velocity value reached.
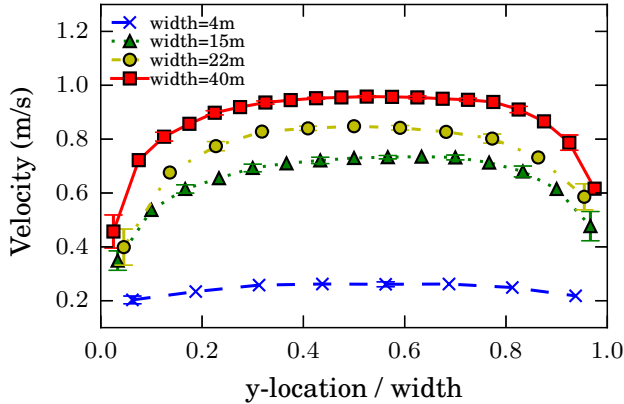

FIG. 5. Velocity profile (velocity vs y-position) for different corridors width (see legend for the corresponding widths). The simulated corridor was 28 m length. Pedestrians walk from left to right with periodic boundary condition in the x-direction. Initially, pedestrians were randomly distributed, the density was $\rho = 6$ in all the cases.

Fig. 6 exhibits the scaled velocity profile. The horizontal axis is normalized by the corresponding corridor width (just like in Fig. 5). In this case, the vertical axis

is normalized by the maximum velocity corresponding to each data set. Filled markers correspond density $\rho = 9$, while empty markers correspond to $\rho = 6$. Notice that all the data follow the same pattern, this suggests that regardless the scale of the corridor (and the density), the velocity profile exhibits a fundamental behavior. Hence, the velocity growth rate from the wall towards the center of the corridor, is the same in spite of the size of the corridor width.
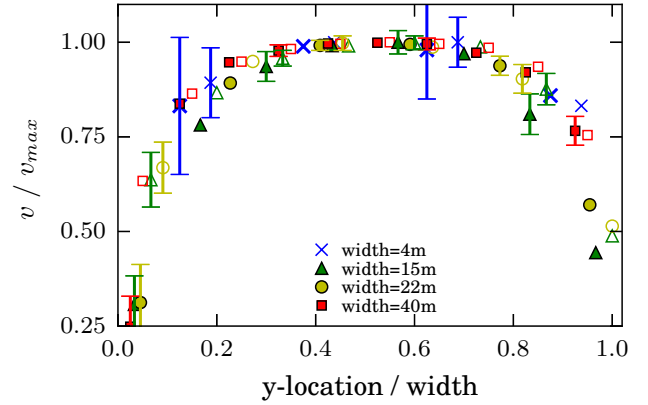

FIG. 6. Scaled velocity profile (normalized velocity) vs. y-location for different corridors width (see legend for the corresponding widths) and two different densities. Empty markers correspond to $\rho = 6$ while filled markers correspond to $\rho = 9$. The simulated corridor was 28 m length. Pedestrians walk from left to right with periodic boundary condition in the x-direction. Initially, pedestrians were randomly distributed. The horizontal axis is normalized by the corridor width, the vertical axis is normalized by the maximum velocity reached in each case.

In this subsection we have shown that the velocity profile has a parabola shape. Pedestrians attain the maximum velocity in the middle of the corridor while the minimum is by the walls. We found out that once normalized by v_{max} and the corridor width, the velocity profile yields a universal behavior (regardless the width of the corridor).

So far we have that narrower corridors produce lower velocities along the corridor. We also learned that the velocity needs to be low enough to avoid the flow increment present in wider corridors. We wonder what is the reason that determines the increase or decrease of the flow in the congested branch. Since the trajectories of pedestrians are straight (there is no crossing path that could reduce the flow), we can hypothesize that the friction force may be the key factor in the flow reduction. This inspired us to analyze the role of the friction coefficient in a simple model for the corridor (see Appendix B).

C. Work done by friction force

In the previous Section we have shown how the velocity takes different values along the corridor. Here we present the spacial distribution of the work done by the friction force. Only the pedestrian-pedestrian friction was calculated.

The work, was numerically calculated using the Trapezoidal rule on each pedestrian. The integration time step was $\Delta t = 0.05$ s. We divided the corridor into a grid with 1 m×1 m cells in order to associate the work values with spacial location. In Fig. 7 we show three heat maps of the absolute value of the work done by the friction force. The horizontal and vertical axis represent the x location and y location of the corridor respectively. The heat map denotes higher work for red color and lower work for blue color. The walls are located at $y = 0$ and $y = w$ (bottom and top of each figure). Fig. 7a corresponds to a 10 m width corridor, Fig. 7b corresponds to a 15 m width corridor and Fig. 7c corresponds to a 22 m width corridor.

In the three figures we observe the same pattern: the regions near the walls (bottom and top) are the regions in which pedestrians suffer the higher work done by the friction. In the center of the corridor the work is reduced in all the cases. Another interesting observation is that the work seems to increase with the corridor width. This happens because in the wide corridors the relative velocity between pedestrians is greater. See Fig. 5 and compare the slopes between the parabolas. It can be seen that the wider the corridor, the greater the slope (corresponding to locations near the wall). As it is stated in Eq.(3), the friction force depends on the compression and the relative velocity among pedestrians. The differences between Figs. 7a, 7b and 7c are only explained by the increment of the relative velocity. The compression levels remain the same in the three cases since the compression only depends on the density (which is fix at $\rho = 6$ for the three heat maps).

In this subsection we have shown that the pedestrians in contact with the wall are the one with the higher work done by friction force.

D. Friction modification

As already mentioned, the results shown so far indicate that friction may be the key to improving the fundamental diagram. We want to make clear that improving the fundamental diagram means obtaining the congested branch reported by different authors, in particular in the Jamaraat study of Helbing et al. where the congested branch reaches a plateau in a 22 m width corridor. The original version of the Social Force Model proposes the same friction coefficient for the
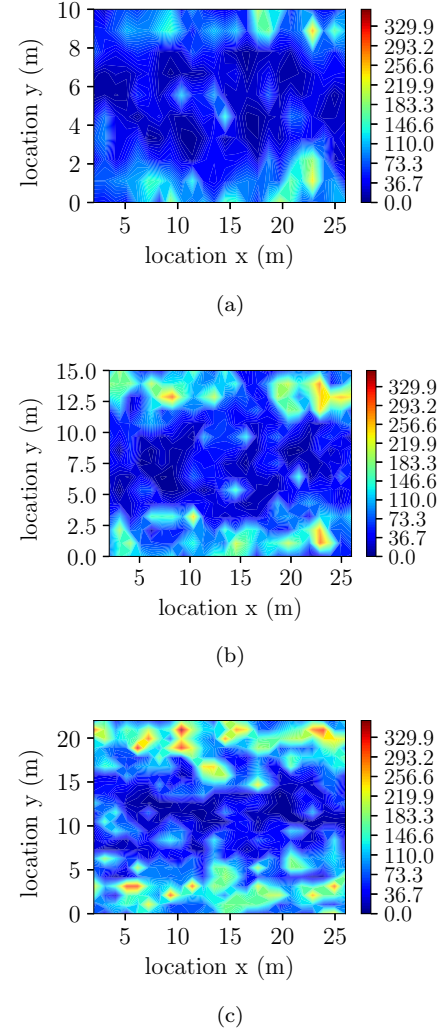
(a)

(b)

(c)

FIG. 7. Heat map for the absolute value of the work done by the friction. The axis represent the location in the corridor (x and y). The scale bar on the right is expressed in J units. The work was numerically integrated with the Trapezoidal rule with $\Delta t = 0.05$ s. The pedestrians desired velocity was $v_d = 1$ m/s. The contour lines were computed on a square grid of 1 m× 1m and then splined to get smooth curves.

pedestrian-pedestrian interaction and the pedestrian-wall interaction. The value proposed was $\kappa = 2.4 \times 10^5$. This value is widely used in many studies despite it lacks a rigorous foundation.

In Appendix B we tested the friction coefficient modification and we found that the fundamental diagram changes its behavior according to the friction coefficient. Analytically, we saw that if the value of κ was properly tuned, the expected fundamental diagram can be achieved. Given this insight, we performed simulations to numerically prove the analytical results. We define κ_i as the friction coefficient of the pedestrian-pedestrian interaction and κ_w as the friction coefficient of the pedestrian-wall interaction. Fig. 8

shows the flow vs density for different values of κ_i and κ_w.

The triangles plot in Fig. 8 correspond to the increment of the wall friction in one order of magnitude (now $\kappa_w = 2.4 \times 10^6$). In this case we left the pedestrian-pedestrian friction unchanged (*i.e.*, $\kappa_i = 2.4 \times 10^5$). We can see that the flow reduces a little bit, but this is not enough to produce the negative slope that characterizes the congested regime.

The circles correspond to a modification of the friction between pedestrians without changing the value of the wall friction. We increased the pedestrian-pedestrian friction by a factor of ten ($\kappa_i = 2.4 \times 10^6$). Here we see a significant reduction of the flow. The qualitative behavior resembles the fundamental diagram reported by Helbing et al. with a well defined congested branch for the greatest densities.

We also tested the case were both friction coefficients are ten times the value of the original model (now $\kappa_w = \kappa_i = 2.4 \times 10^6$). The squared symbols represent this scenario. As expected, the flow reduces significantly respect the original case (cross symbol plot). Interestingly, the reduction of the flow is more than the reduction due to the increment of κ_i plus the reduction of the flow due to κ_w. This behavior is indicative that the superposition principle does not hold in this system because of the non-linearity of the equation of motion.

This finding allows us to affirm that the friction plays a crucial role in the functional behavior of the fundamental diagram. The increment of both individual-individual friction and wall friction are determinant in order to achieve a congested branch. Other authors address the 'congested regime problem' by modifying different aspects of the model. Parisi et al. impose zero desired velocity once pedestrians are close enough [16], Johannson increases the relaxation time in order to slow down the net-time headway Ref. [18] and more recently, Kwak et al. in Ref. [15] induce the jamming transition by an attraction. Our results show that the empirical behavior for the fundamental diagram can be achieved by properly increasing the friction coefficients. In Appendix A we discuss about how the modification of the relaxation time and the increment of the friction coefficient yield the same effect, since they affect the same term in the reduced-in-units equation of motion.

We argue that in real scenarios, a combination of all these factors may be the cause of the marked flow reduction that portray the fundamental diagram. The pedestrians path can be very complex even if it is a simple enclosure (straight corridor) and the target is well defined (unidirectional flow). Beyond the complexities given by the internal motivations of pedestrians, we strongly suggest studying and modeling coefficients of friction between individuals and the friction with the

walls. These two parameters have shown to be very important in the pedestrian dynamics and deserve a closer inspection in future research.

We want to emphasize that the proposals stated in Refs. [15, 16, 18] only apply under normal conditions. If a crowd is under high levels of anxiety (*i.e.* panic), pedestrians will not keep distance with each other nor will feel the urge to see an "attraction". The only goal in an evacuation under panic is to leave the room. Thus, studying the friction coefficients may be a critical factor to properly reproduce the dynamics of a massive evacuation under stress.

With all these insights, we can say that the narrow corridors have no problems with the flow vs. density relation because they do not allow pedestrians to reach high velocities. This happens because in narrow corridors, the friction of the walls has a lot of 'relative weight' in the overall friction of the system. The friction exerted by the walls is fundamental in order to produce the parabolic shape of the velocity profile. The walls provide friction force in the opposite direction to the speed of the individual (drag backwards), since they act like a fixed pedestrian. In other ways, friction between pedestrians can produce either drag forward or drag backwards depending on the the contacting pedestrians velocities (see Eq. 3).
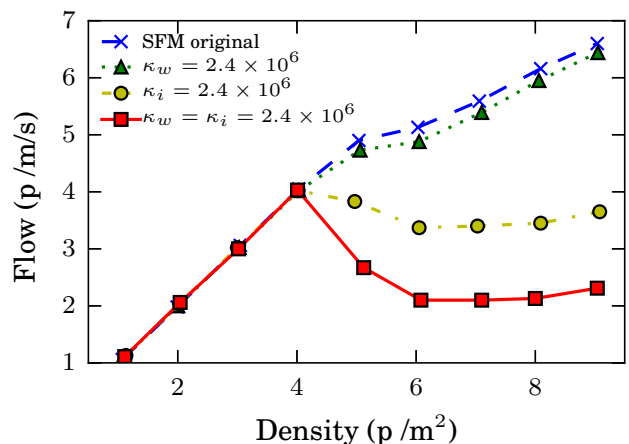

FIG. 8. Fundamental diagram (flow vs density) for different friction coefficient (see legend for the corresponding values). The simulated corridor was 28 m length. Pedestrians walk from left to right with periodic boundary condition in the x-direction. Initially, pedestrians were randomly distributed. For each density, we measure the flow once the system reaches the stationary state.

In this subsection we have shown that an adequate modification of the friction coefficients yields a fundamental diagram with the qualitative behavior reported in empirical measurements (with the flow reduction for

the greatest densities). We have also discussed different approaches proposed by other authors in order to attain this problem. See Appendix A for a more detailed discussion.

E. Clusters

Cluster formation is a very important process in pedestrian dynamics. Moreover, is the key process that explains the clogging phenomena in bottleneck evacuations. We analyzed the clustering formation according to the granular cluster definition given in [3] In Fig. 9 we show the histogram of the cluster size distribution for three different densities, from top to bottom: $\rho = 4.5$, $\rho = 5$ and $\rho = 5.5$. we have chosen these three values as lower densities yield to non-clustered arrangements and higher densities yield a unique giant cluster. For each density we studied two situations. The cluster size distribution for the original parameters of the Social Force Model (left hand side plots) and the cluster size distribution corresponding to the increment of the friction coefficients by a factor of ten (right hand side plots).

We found a couple of intriguing results. Incrementing the density produces bigger size clusters until it reaches a critical value in which the size distribution shifts to a bimodal distribution (compare 9c with 9e and 9b with 9d). Once this phenomena takes place, there are only two possibilities for the clusters: either they are small sized clusters caged in the crowd or is a giant cluster (with a size comparable with the entire crowd).

We also found that this phenomena is prompted by the friction. If the friction is higher, the transition to the bimodal distribution takes place for lower density values. See Fig. 9c and Fig. 9d. Despite the fact that both correspond to the same density, 9d already attained the bimodal distribution since the friction force is ten times greater than 9c. This peculiar phenomenon occurs because when there is more friction, individuals find it more difficult to detach from each other. In the opposite case, when the friction is low, the individuals detach themselves more easily, leading to a situation where large clusters are less probable.

To understand the full picture, in Fig. 10 we show the fraction of clustered individual as a function of the density for four different situations in which we change the friction coefficients. The fraction of clustered individuals is defined as the amount of pedestrians that belong to a cluster over the total number pedestrians in the corridor. We can see that there is a transition from a non-clustered crowd to a full-clustered crowd. This transition occurs in a very limited range of densities, causing the process of cluster formation to occur for $4.4 < \rho < 5.3$. When the friction coefficient is high,
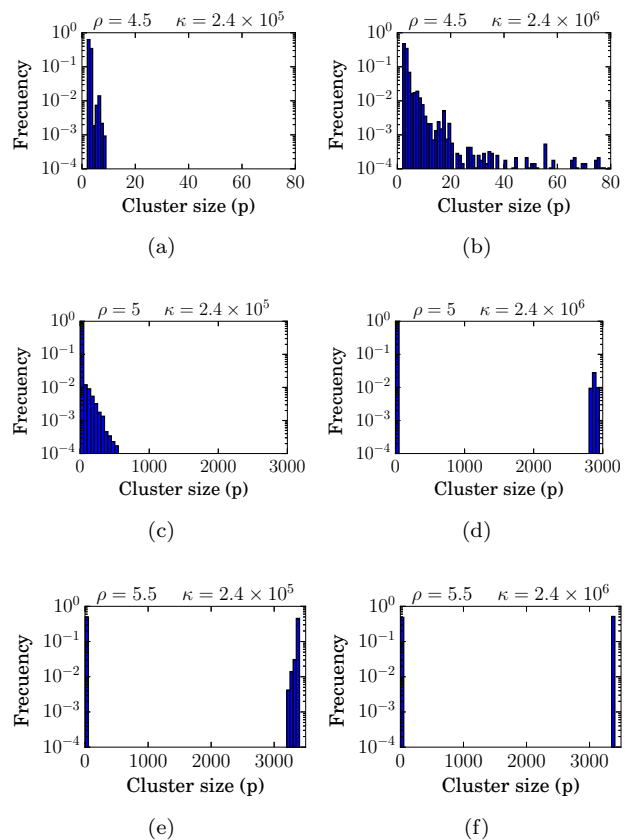

FIG. 9. Cluster size distribution for six different scenarios. (a) SFM friction parameters and $\rho = 4.5$, the bin size is 1 p (b) friction parameters increased by a factor of ten and $\rho = 4.5$, the bin size is 1 p (c) SFM friction parameters and $\rho = 5$, the bin size is 50 p (d) friction parameters increased by a factor of ten and $\rho = 5$, the bin size is 50 p (e) SFM friction parameters and $\rho = 5.5$, the bin size is 50 p (f) friction parameters increased by a factor of ten and $\rho = 5.5$, the bin size is 50 p.

the transition takes place for lower density values. This result is consistent with the histograms shown in Fig .9, supporting the fact that friction promotes the formation of clusters.

As expected, the transition becomes more abrupt when both κ_i and κ_w are incremented (squared symbol plot). When only one of those two coefficients is incremented, the fraction of clustered individuals is greater than the original model. Notice that there is not a big difference between the modification of κ_i and the modification of κ_w. This suggests that it does not matter if the clusterization begins to take place in the areas near the walls or in the middle of the crowd.

In this section we have proved that the clustering process can be prompted by incrementing the friction coefficient. Both the size of the clusters and the fraction of clustered individuals increase with friction and density.
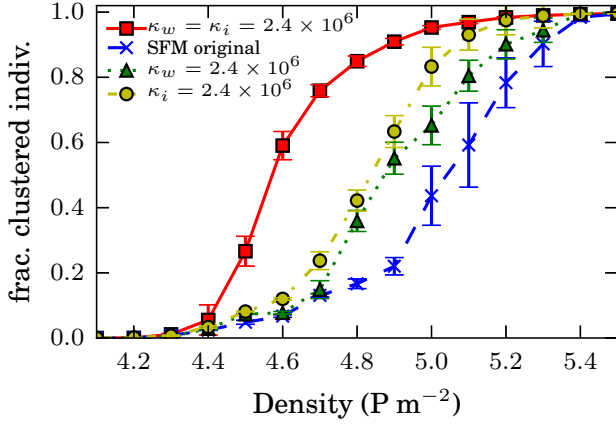
FIG. 10. Fraction of clusterized individuals as a function of the density. Square symbol correspond to $\kappa_w = \kappa_i = 2.4\times10^6$, circles to $\kappa_i = 2.4 \times 10^6$ and $\kappa_w = 2.4 \times 10^5$, triangles to to $\kappa_i = 2.4 \times 10^5$ and $\kappa_w = 2.4 \times 10^6$ and crosses to the coefficients of the original Social Force model ($\kappa_i = 2.4 \times 10^5$ and $\kappa_w = 2.4 \times 10^5$). The pedestrians walk across a corridor with $v_d = 1$m/s. The measurements were recorded every 0.5 s once the system reaches the stationary state. The values corresponding to the fraction of clustered individuals were averaged over 170 s. The cluster cutoff distance was 0.46 m (equivalent to the shoulders width of the pedestrians).

V. CONCLUSIONS

Our investigation focused on the fundamental diagram in the context of the social force model. We took a particular case of study (pilgrimage of the entrance to the Jamaraat bridge) to compare the numerical simulation results with the empirical results measured by Helbing and co-workers. We found out that the social force model in its original fashion is not capable of reproducing the fundamental diagram since the flow increases even for overcrowded scenarios. Using analytical techniques we discovered that either increasing the friction coefficient or increasing the relaxation time may be the key to achieving a non-increasing flow in the congested regime of the fundamental diagram. The second approach was the one implemented by Johansson and a similar idea was introduced in Ref.[16]. We proved that both approaches are equivalent since both of them affect in the same way, the same term of the reduced-in-units equation of motion.

The analytical schematic model suggests that the problem could be addressed by modifying the friction coefficient. In light of this, we performed numerical simulations increasing κ and attained the fundamental diagram behavior reported in the empirical measurements.

When exploring the velocity profile, we found that it has a parabolic shape. Pedestrians reach the maximum velocity in the middle of the corridor while the minimum is by the walls. We found out that once scaled by v_{max} and the corridor width, the velocity profile yields a universal behavior (regardless the width of the corridor).

The presence of clustering structures was found to be prompted by the increment of the friction coefficient. Interestingly, increasing the pedestrian-pedestrian friction (κ_i) or the pedestrian-wall friction coefficient (κ_w) yields a similar clusterization dependence with density.

The phenomena reported in this paper suggests that further research needs to be done regarding the friction coefficient. We propose modeling the pedestrian-wall friction interaction with a different coefficient than the pedestrian-pedestrian friction interaction. We want to stress the fact that studying the friction coefficients may be a critical factor to properly reproduce the dynamics of a massive evacuation under high levels of anxiety.

Appendix A: The reduced equation of motion

The equation of motion within the context of the Social Force Model includes at least six parameters (m, τ, A, B, κ and v_d), but the equation itself barely depends on two. The process of parameter's reduction is achieved by defining the (reduced) magnitudes

$$\begin{cases} t' &= t/\tau \\ r' &= r/B \\ v' &= v/v_d \end{cases} \quad (A1)$$

The (reduced) equation of motion reads

$$\frac{d\mathbf{v}'}{dt'} = \frac{\tau}{m\,v_d}\left(\mathbf{f}_d + \mathbf{f}_s + \mathbf{f}_g\right) \quad (A2)$$

It is straight forward from Eq. (A2) that the corresponding reduced forces can be defined as follows

$$\begin{cases} \mathbf{f}'_d &= \hat{\mathbf{e}}_d - \mathbf{v}' \\[2mm] \mathbf{f}'_s &= \mathcal{A}\exp(r' - d')\,\hat{\mathbf{n}} \\[2mm] \mathbf{f}'_g &= \mathcal{K}\,(2r' - d')\,\Theta(2r' - d')\,(\Delta\mathbf{v}' \cdot \hat{\mathbf{t}})\,,\hat{\mathbf{t}} \end{cases} \quad (A3)$$

where $\mathcal{A} = A\tau/(m\,v_d)$ and $\mathcal{K} = \kappa B\tau/m$.

Notice that $\mathcal{A}$ and $\mathcal{K}$ are actually the only two control parameters in Eq. (A2) for identical pedestrians. The ratio τ/m is common to both, but the magnitudes Av_d^{-1} and κB handle each parameter separately.

The fact that $\mathcal{A}$ and $\mathcal{K}$ share the parameter τ is in agreement with the conclusions outlined in Ref. [18]. The relaxation time (or "net-time headway") τ actually "weights" the effects of the environment on the individual (that is, the social repulsion and the friction), and thus, appears as a "key control parameter" for the fundamental diagram as claimed in Ref. [18].

The role of τ may be somewhat ambiguous whenever the social repulsion becomes negligible with respect to the friction. This may occur if some kind of balance exists between neighboring pedestrians in symmetrical configurations (*i.e.* in crowded corridors). We may hypothesize that the "key control parameter" may correspond to either τ, or, the friction itself κ. This is an open question, and a first order approach to this matter is outlined in Section B.

Appendix B: A simple model for the corridor

A toy model for a moving crowd along a corridor is the one represented schematically in Fig. 11. Pedestrians (circles in Fig. 11) are assumed to be lined up from side to side across the corridor, at any given position. Social forces in the x-direction are further considered to vanish because of translational symmetry. Thus, only the sliding friction is allowed to balance the the pedestrians own desire. The (reduced) movement equation for the x-direction according to Section A and Fig. 11 is
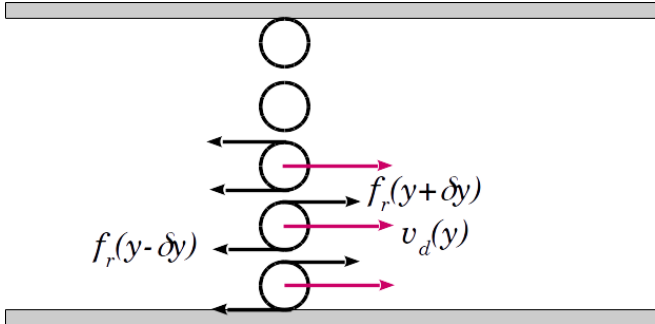

FIG. 11. Schematic diagram for individuals in a corridor. The circles represent pedestrians moving from left to right. The desired force (red arrows) and sliding friction (black arrows) are assumed to be the only relevant forces.

$$\frac{dv'}{dt'}(y') = 1 - v'(y') + f'_g(y' + \delta y') - f'_g(y' - \delta y') \quad \text{(B1)}$$

where $v'(y')$ corresponds to the (reduced) velocity (for the x-direction) of the individual located at the y' position. Notice that the individuals remain at the same y' position while traveling through the corridor, since balance is expected to take place across the corridor. These positions are roughly $\delta y'$, $3.\delta y'$, $5.\delta y'$,.... Actually, it is not relevant (for now) the value of y', and a further simplification can be done by labeling $v'(y') = v_i$ and $v'(y' \pm 2.\delta y') = v_{i\pm 1}$. The velocity of the individual in contact with the bottom wall in Fig. 11 will be labeled as v_1.

The last two terms in Eq. (B1) correspond to the net drag applied on the pedestrian with velocity v_i. According to Eq. (A3) this drag may be expressed as

$$f'_{g,i+\frac{1}{2}} - f'_{g,i-\frac{1}{2}} = \begin{cases} 2\alpha\,v_2 - 3\alpha\,v_1 & i = 1 \\ 2\alpha\,(v_{i+1} - 2v_i + v_{i-1}) & i > 1 \end{cases} \quad \text{(B2)}$$

for $\alpha = \mathcal{K}(r' - \delta y')$. Recall that our first order approach considers $\delta y'$ as roughly uniform across the corridor.

The stationary situation can be computed straight forward from Eq. (B1). Thus, for $\dot{v}_i = 0$ the following set of equations determine the velocity profile in the corridor (within this toy model)

$$\begin{cases} (3\alpha + 1)\,v_1 - 2\alpha\,v_2 & = 1 \\ -2\alpha\,v_{i-1} + (4\alpha + 1)\,v_i - 2\alpha\,v_{i+1} & = 1 \end{cases} \quad \text{(B3)}$$

Notice from Eq. (B2) that $\alpha = 0$ means no friction at all, and thus, the individuals are allowed to move free from drag. It can be verified that $v_i = 1$ solves the set (B3) for this scenario. The $\alpha = 0$ scenario is expected to occur, however, for densities below a contacting threshold.

A boundary condition needs to be imposed in order to solve Eqs. (B3) for $\alpha \neq 0$. We fix $v_i = v_{i+1}$ at the middle of the corridor since the velocity profile should be specularly distributed with respect to the mid-axis of the corridor. Fig. 12 shows the computed mean velocity for the bottom side profile as function of α.

Fig. 12 exhibits a decreasing behavior for increasing values of α. As explained above, the maximum value occurs at $\alpha = 0$ (*i.e.* $\langle v_i \rangle = 1$). However, the decreasing slope slows down for increasing number of individuals. This corresponds to a flattening in the velocity profile, (see Section IV for details).

The mean flux of individuals can be built from the mean velocity and the corresponding pedestrian density as follows
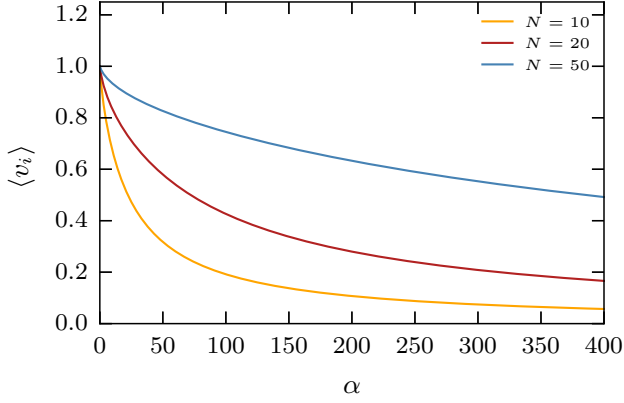
FIG. 12. Mean velocity of the bottom half of the individuals vs. the parameter α. Both axis are dimensionless. N corresponds to the number of individuals.

$$J = \begin{cases} \rho & \text{for } \alpha = 0 \\ (\rho_0 + c\,\alpha)\,\langle v_i \rangle & \text{for } \alpha > 0 \end{cases} \quad (B4)$$

where $\langle v_i \rangle$ equals unity for the case $\alpha = 0$, and thus, it was omitted in (B4). The density $\rho = \rho_0 + c\,\alpha$ corresponds to the packing density (that, the density above the contacting threshold) and c corresponds to a somewhat "packing coefficient". Fig. 13 shows the flow as a function of the density, assuming $\rho_0 = 1$ for simplicity.
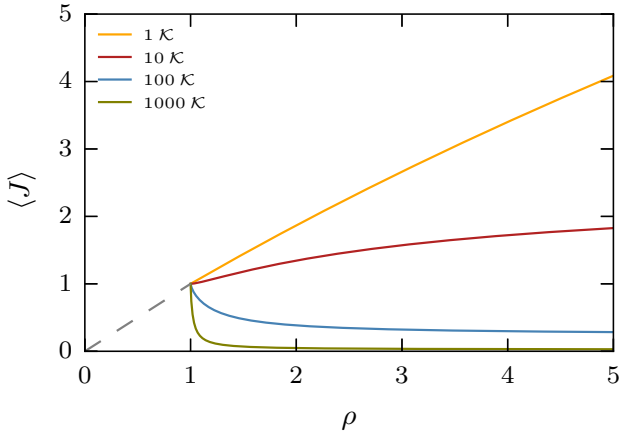

FIG. 13. Mean flux of the bottom half of the individuals vs. the pedestrian (global) density ρ (see text for details). Both axis are dimensionless. The number of individuals across the corridor was set to $N = 10$, and the contacting threshold was set to $\rho_0 = 1$. The dashed line corresponds to the flux at the low density regime (say, $\langle v_i \rangle = 1$).

The pedestrian flux J attains two possible behav-

iors, according to Fig. 13. For packing coefficients $c < 0.05$, the flux diminishes as the corridor becomes more crowded. But, if c surpasses this threshold, the flux slope becomes positive, although the mean velocity diminishes. We conclude that the role of the pedestrians' friction coefficient is crucial for building the fundamental diagram.

Appendix C: Testing out previous results

In this Appendix we show that the friction modification does not alter characteristic behaviors of pedestrian dynamics. In order to check this out, we performed numerical simulations of a room of 225 pedestrian escaping through a narrow door (bottleneck enclosure). The evacuation time (clearance time) t_e is a function of the desired velocity v_d. This function has a minimum such that below it, t_e is a decreasing function of v_d while above, the tendency is reversed. It means that the evacuation process is optimum at moderated v_d. This is a well known phenomena called the Faster-is-slower effect. This effect was reported in numerical simulations [1, 6] and it has also experimental support [26].

In Fig. 14 we show the evacuation time as a function of the desired velocity corresponding to a friction coefficient ten times grater than the friction coefficient of the original Social Force Model (i.e. now $\kappa = 2.4 \times 10^6$). We can see that this modification preserves the Faster-is-slower effect. The inset exhibits the evacuation time as a function of the desired velocity with the friction coefficient of the original model ($\kappa = 2.4 \times 10^5$).

Another pedestrian dynamics phenomena is the lane formation reported in bidirectional flows [27–30]. This means, individuals spontaneously organize in lanes of uniform walking direction, if the pedestrian density is high enough. One of the major achievements of the Social Force Model is its ability to reproducing this emergent phenomena in which the microscopic interactions between pedestrians is enough to produce a global pattern. We run bidirectional flow simulation and verified that the friction increment still reproduces the lane formation process.

Fig. 15 exhibits the quotient (rate) between the evacuation time with the friction modification and the evacuation time of the original model. This quotient is a function of the desired velocity. As the desired velocity increases, the rate of evacuation times approaches a constant value ~ 9. This result is consistent with the formula (9) in the work of Ref.[25]. The friction force becomes dominant in the range of high desired velocity since it promotes the collisions between pedestrians. In this regime, the Ec. (9) of Ref.[25] becomes a good approximation of the evacuation time. Thus, it is reasonable that dividing t_e (for the friction incremented) by t_e (with the original friction value) yields a constant value
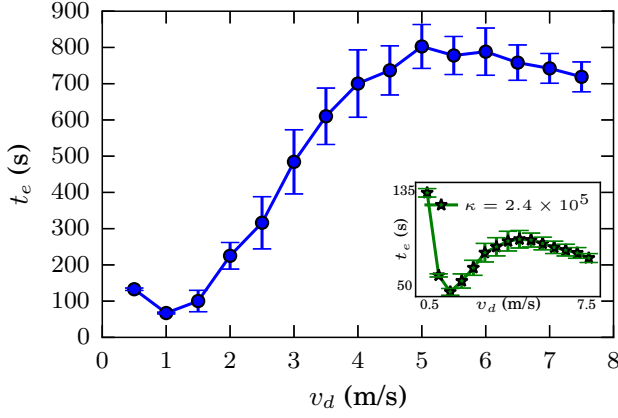
FIG. 14. Mean evacuation time (seconds) vs. the pedestrians desired velocity (m/s). The room was 20 m × 20 m size. Mean values were computed from 30 evacuation processes. The pedestrians were initially placed in a regular square arrangement along the room with random velocities, resembling a Gaussian distribution with null mean value. The friction coefficient was $\kappa = 2.4 \times 10^6$. The inset shows the evacuation time vs the desired velocity for the friction coefficient corresponding to the original model ($\kappa = 2.4 \times 10^5$).
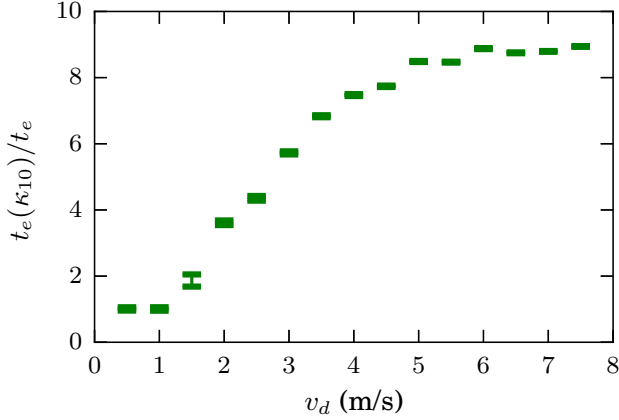
for high v_d.

FIG. 15. Rate of evacuation time ($t_e(\kappa_{10})/t_e$) vs the desired velocity. The room was 20 m × 20 m size. Mean values were computed from 30 evacuation processes. The pedestrians were initially placed in a regular square arrangement along the room with random velocities, resembling a Gaussian distribution with null mean value. The friction coefficient was $\kappa = 2.4 \times 10^6$.

We also tested the situation in which $k_i = 2.4 \times 10^6$ and $k_w = 0$. We obtained similar results to the one obtained when $k_i = k_w = 2.4 \times 10^6$ because in bottleneck evacuations the friction of the walls do not play a fundamental role in the evacuation process.

[1] D. Helbing, I. Farkas, and T. Vicsek, Nature **407**, 487 (2000).

[2] D. Helbing and P. Molnár, Physical Review E **51**, 4282 (1995).

[3] D. Parisi and C. O. Dorso, Physica A **354**, 606 (2005).

[4] D. Parisi and C. O. Dorso, Physica A **385**, 343 (2007).

[5] G. Frank and C. O. Dorso, Physica A **390**, 2135 (2011).

[6] I. Sticco, G. Frank, S. Cerrotta, and C. Dorso, Physica

A: Statistical Mechanics and its Applications **474**, 172 (2017).

[7] G. Frank and C. O. Dorso, International Journal of Modern Physics C **26**, 1 (2015).

[8] G. Frank and C. Dorso, International Journal of Modern Physics C **27**, 1 (2016).

[9] F. Cornes, G. Frank, and C. Dorso, Physica A: Statistical Mechanics and its Applications **484**, 282 (2017).

[10] T. I. Lakoba, D. J. Kaup, and N. M. Finkelstein, Simulation **81**, 339 (2005).

[11] D. Helbing, A. Johansson, and H. Z. Al-Abideen, Physical review E **75**, 046109 (2007).

[12] A. Seyfried, M. Boltes, J. Kähler, W. Klingsch, A. Portz, T. Rupprecht, A. Schadschneider, B. Steffen, and A. Winkens, in *Pedestrian and Evacuation Dynamics 2008*, edited by W. W. F. Klingsch, C. Rogsch, A. Schadschneider, and M. Schreckenberg (Springer Berlin Heidelberg, Berlin, Heidelberg, 2010) pp. 145–156.

[13] A. Seyfried, B. Steffen, W. Klingsch, and M. Boltes, Journal of Statistical Mechanics: Theory and Experiment **2005**, P10002 (2005).

[14] A. Johansson, D. Helbing, and P. K. Shukla, Advances in Complex Systems **10**, 271 (2007).

[15] J. Kwak, H.-H. Jo, T. Luttinen, and I. Kosonen, Physical Review E **96**, 022319 (2017).

[16] D. R. Parisi, M. Gilman, and H. Moldovan, Physica A: Statistical Mechanics and its Applications **388**, 3600 (2009).

[17] A. Seyfried, B. Steffen, and T. Lippert, Physica A: Statistical Mechanics and its Applications **368**, 232 (2006).

[18] A. Johansson, Phys. Rev. E **80**, 026120 (2009).

[19] R. A. Smith and J. Dickie, "Engineering for crowd safety," (1993).

[20] M. Mōri and H. Tsukaguchi, Transportation Research Part A: General **21**, 223 (1987).

[21] A. Polus, J. L. Schofer, and A. Ushpiz, Journal of transportation engineering **109**, 46 (1983).

[22] A. Jelić, C. Appert-Rolland, S. Lemercier, and J. Pettré, Physical Review E **85**, 036111 (2012).

[23] D. Littlefield, *Metric handbook* (Routledge, 2008).

[24] S. Plimpton, Journal of Computational Physics **117**, 1 (1995).

[25] I. Sticco, F. Cornes, G. Frank, and C. Dorso, Physical Review E **96**, 052303 (2017).

[26] J. M. Pastor, A. Garcimartín, P. A. Gago, J. P. Peralta, C. Martín-Gómez, L. M. Ferrer, D. Maza, D. R. Parisi, L. A. Pugnaloni, and I. Zuriguel, Phys. Rev. E **92**, 062817 (2015).

[27] C. Feliciani and K. Nishinari, Physical Review E **94**, 032304 (2016).

[28] D. Helbing, P. Molnár, I. J. Farkas, and K. Bolay, Environment and planning B: planning and design **28**, 361 (2001).

[29] W. Guo, X. Wang, and X. Zheng, Physica A: Statistical Mechanics and its Applications **432**, 87 (2015).

[30] J. Qiao, L. Sun, S. Qiu, J. Rong, and X. Liu, Promet-Traffic&Transportation **29**, 489 (2017).